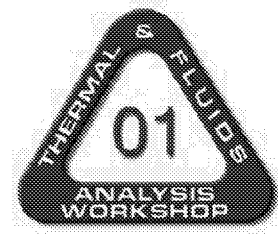


CORRECTIONS OF HEAT FLUX MEASUREMENTS ON LAUNCH VEHICLES



Dr. Thomas R. Reinarts

Monique L. Matson

Laurie K. Walls

NASA / ELV Mission Analysis Branch

VB – A3

Kennedy Space Center, Florida 32899

ABSTRACT

Knowledge of aerothermally induced convective heat transfer is important in the design of thermal protection systems for launch vehicles. Aerothermal models are typically calibrated via the data from circular, in-flight, flush-mounted surface heat flux gauges exposed to the thermal and velocity boundary layers of the external flow. Typically, copper or aluminum Schmidt-Boelter gauges, which take advantage of the one-dimensional Fourier's law of heat conduction, are used to measure the incident heat flux. This instrumentation, when surrounded by low-conductivity insulation, has a wall temperature significantly lower than the insulation. As a result of this substantial disturbance to the thermal boundary layer, the heat flux incident on the gauge tends to be considerably higher than it would have been on the insulation had the calorimeter not been there. In addition, radial conductive heat transfer from the hotter insulation can cause the calorimeter to indicate heat fluxes higher than actual. An overview of an effort to develop and calibrate gauge correction techniques for both of these effects will be presented.

INTRODUCTION

An instrument placed into a system to measure a given effect changes the environment simply by its addition to the system. Therefore, the measured value deviates by some amount from the undisturbed value, and it is important to understand the magnitude of this deviation. The deviation is small for many types of measurements, but can be substantial for heat flux gauges on launch vehicles. Since analytical models used to predict heat flux loads on launch vehicles are frequently calibrated by in-flight measurements from heat flux gauges, it is important to understand the contributing factors to sensor disturbance of the environment and its impact on sensor measurements. In areas with TPS, the dominating contributor is the potentially large temperature difference between the hotter, low conductivity insulation that surrounds the cooler gauge. This results in an incident heat flux indicated by the gauge that is higher than it would be on the insulation if the gauge had not been introduced into the system, potentially by factors of two or more. There are two causes of this (Figure 1). First, the near step change in wall temperature from TPS to sensor disturbs the thermal boundary layer, producing a higher incident flux on the sensor^{1,2}. Second, the lower temperature gauge also acts as a heat sink, causing a

radial flow of energy through the sides of the gauge that moves through the epoxy/wafer and down the gauge body, which increases the indication of surface normal incident heat flux.

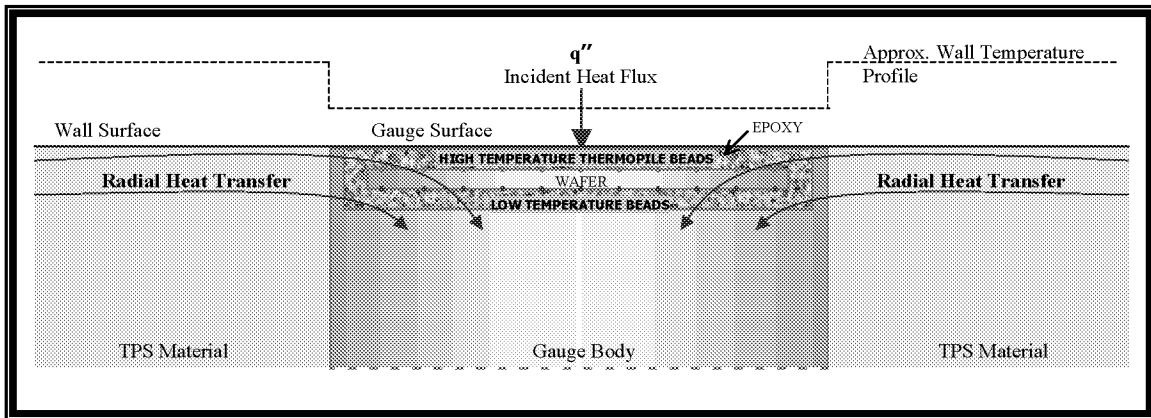


Figure 1: Diagram of Heat Transfer through a Schmidt-Boelter Gauge

An effort to quantify these effects has been undertaken in a three-part study, which includes modeling of the external velocity and temperature boundary layers, modeling of the conductive heat transfer within the sensor and from the surrounding TPS to the sensor, and testing in an aerothermal facility at Marshall Space Flight Center (MSFC). The overall modeling and calibration effort will eventually be used to quantify and correct the in-flight sensor errors. The expected result is an improved understanding of aerothermally induced convective heat transfer on launch vehicles, reduced design loads, and relaxed TPS requirements. While current data provide conservative factors of safety, there are potential benefits attainable from reduced conservatism via lower TPS mass and reduced TPS application requirements.

BOUNDARY LAYER ANALYSIS

In convective flow, dramatic thermal boundary layer changes can result from steep surface thermal gradients in the direction of flow. The heat transfer from a convective flow to the plate can be described by the following equation:

$$(1) \quad q'' = -k_f \nabla T_{f0}$$

where k_f is the thermal conductivity of the fluid, T_{f0} is the temperature of the fluid, and q'' is the fluid/wall heat-flux.

Thus, a dramatic change in wall surface temperature results in a change in the fluid thermal gradient at the wall interface, causing a changed heat flux into the wall. Schmidt-Boelter gauges are typically made of materials with relatively high specific heat and high thermal conductivity. When surrounded by a TPS with low conductivity, the surface temperature gradient from TPS to gauge can be steep. In this situation, the heat flux into the gauge is not the same as the heat flux into the same area if the gauge is not present. Attempts at modeling this phenomenon has been

performed by others^{1,2,3,4}. These models assumed a step change in wall temperature, and constant fluid properties over the surface temperature gradients. A CFD effort has been undertaken to include fluid property variations and calculate the difference between the gauge incident and undisturbed heat fluxes.

Referencing Figure 2, the magnitude of this dissimilar material effect is dependent on fluid properties, flow conditions at the leading edge, flow development length, calorimeter size, and of course, the surface temperature gradient.

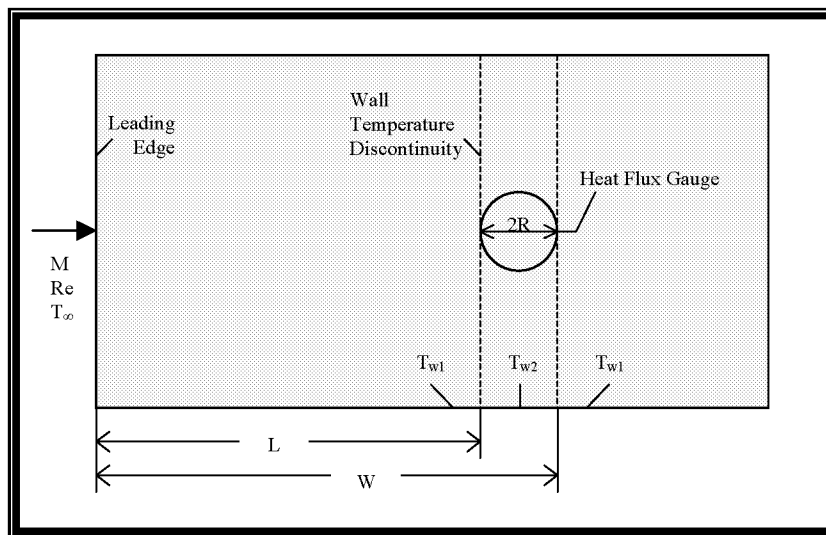


Figure 2: Diagram of CFD 2-D Plate Model

CONDUCTIVE HEAT TRANSFER ANALYSIS

In addition to boundary layer effects, hotter surrounding TPS can conduct energy into the calorimeter and cause the calorimeter to indicate a higher than actual surface incident heat flux. To understand the conductive heat transfer effects on a Schmidt-Boelter gauge, it is important to also understand the operation and construction of the gauge. The Schmidt-Boelter gauge includes a coiling of thermopile wire around a wafer, which is encased by a low conductivity epoxy. The thermopile beads are located on the top (high temperature thermopile) and bottom (low temperature thermopile) of the wafer surface. These thermopile beads provide a temperature gradient that, based on appropriate calibration and the one-dimensional Fourier's law of heat conduction (Equation 2), outputs the incident heat flux.

$$(2) \quad q'' \propto \frac{\delta T}{\delta x}$$

Fourier states that, for steady state one-dimensional heat transfer through a given homogenous material, the heat flux, q'' , is directly proportional to the differential temperature, δT , divided by the differential length, δx . Since the gauge's operation is based on this temperature difference

between the upper and lower surface of the wafer, the radial heat transfer directly increases the incident heat flux measurement. Previous models have been developed to study sensitivity and to assist in gauge design⁵. Yet, to the authors' knowledge, an investigation of the radial effects has not been pursued before. A detailed description of Schmidt-Boelter gauge design/operation can be found in Carl Kidd's AEDC report⁵. The design and development of the three-dimensional Schmidt-Boelter gauge model is presented next.

SCHMIDT-BOELTER MODEL DESIGN AND DEVELOPMENT

A Schmidt-Boelter (S-B) gauge comprises four major components, including the cylindrical conductive gauge body, the non-conductive epoxy, the conductive rectangular wafer and the thermopile (Figure 3). Note that the gauge body and the wafer are typically composed of the same conductive material, usually copper or aluminum.

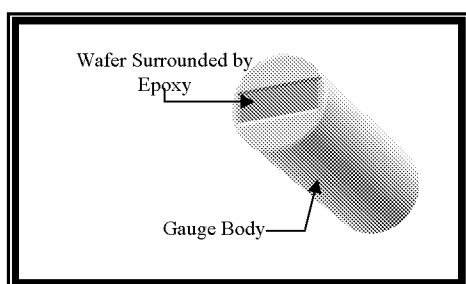


Figure 3: Basic Diagram of S-B Gauge

The gauge measures the temperature difference between the top and bottom surfaces of the wafer via the thermopile, outputting a signal proportional to the incident heat flux. The epoxy is exposed to the top surface of the gauge and completely encases the wafer and thermocouple wire. The idealizations incorporated by this 3-D model are shown in the figure below. Note that the thermocouple wire and beads are shown for explanation purposes only (Figure 4). Kidd analyzed the effects of the size and

material of the thermocouple wire on heat transfer measurements, which show that wire having diameters less than 0.003 in (0.0762 mm) induce small errors⁶. Therefore, they are considered negligible for modeling construction because of their limited impact on the overall thermal environment.

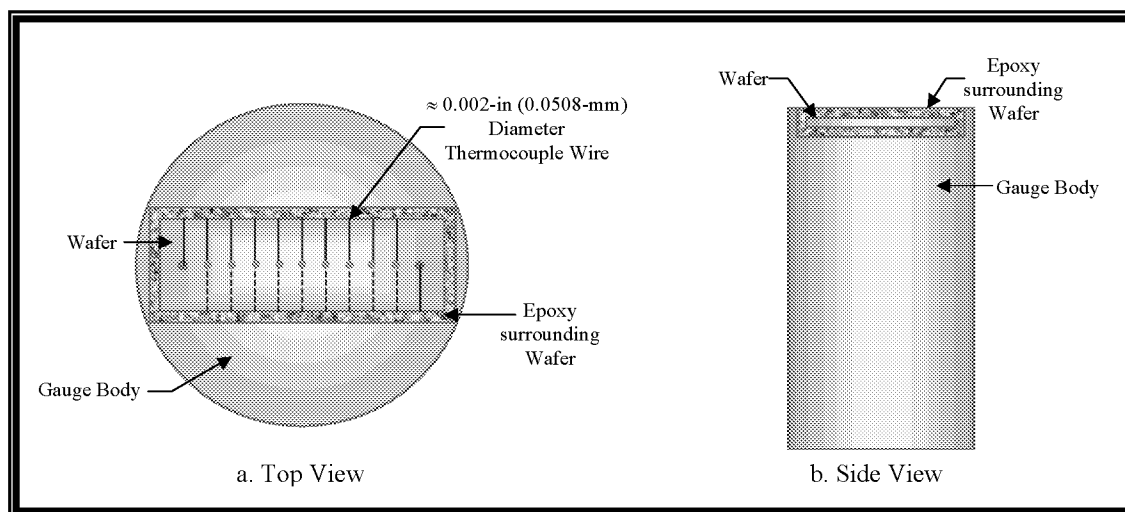


Figure 4: Idealization used for Modeling of the S-B Gauge

The software used to develop and analyze this model was SINDA/G 2.1, a finite-differencing thermal analyzer. Each node was manually generated in order to provide a customized model that focuses on the temperature differences measured by the gauge. The 3-D Schmidt-Boelter gauge model consists of over 3600 nodes, the densest mesh being in the epoxy/wafer area. There is a high concentration of detail there because the effect on the epoxy/wafer is the focus of this radial heat transfer study. Less detail is needed for those nodes that are composed of the same material and are not located near the relative vicinity of the wafer.

AEROTHERMAL TESTING AT MARSHALL SPACE FLIGHT CENTER

Both the CFD and the detailed gauge model calibrations will be achieved via testing of flat plates with thin skin calorimeters and copper and aluminum Schmidt-Boelter gauges. The thin skin calorimeters will indicate the actual heat flux, and the Schmidt-Boelter gauges will give readings that, when properly corrected by the calibrated models, will match the thin skin measurements. Test panels are shown in Figure 5 (Page 6), and will be tested in the Improved Hot Gas Facility (IGHF) at MSFC. Note that the diagrams are not to scale but the panels are 12 inches by 19 inches. There are two categories of test panels: with TPS and without TPS.

Three panels of different materials without TPS will be used. The materials include stainless steel, copper, and aluminum. Each will include one thin skin calorimeter of a material similar to the plate. The stainless steel panel will include two more thin skin calorimeters on the same flow path line as the first to determine incident heat rate variations as a function of location along the major plate axis. Each of these plates will also have two Schmidt-Boelter calorimeters of dissimilar materials, located as shown in Figure 5. The thin skin gauges will be made of the same material as the plate and will give an accurate assessment of the incident convective heat flux.

The fourth panel will be stainless steel, partially covered by an ablative, low thermal conductivity material (also shown in Figure 5). The ablative material will most likely be BTA, and will appear as rectangular strips on either side of a stainless steel strip centered and in the direction of flow. The ablative material will be approximately 0.125 in thick, and the stainless steel below the TPS will be machined out so the BTA is level with the center strip of stainless steel. Three thin skin calorimeters will be used, and will appear as in the stainless steel panel with no TPS. One copper and one aluminum S-B gauge will appear flush mounted with the TPS, each on a separate TPS strip. The TPS will be cured with the S-B's in situ, with no gap between the gauge and the TPS.

Summarizing, four different panels have been designed and are in fabrication: 1) a copper panel with one copper S-B gauge, two aluminum S-B gauges, and a thin skin calorimeter; 2) an aluminum panel with one aluminum S-B gauge, two copper S-B gauges, and one thin skin calorimeter; 3) a stainless steel panel with three thin skins, one copper S-B gauge, and one aluminum gauge; and 4) a stainless steel panel partially covered with an ablative with three thin skins, one copper S-B gauge, and one aluminum S-B gauge. The copper gauges are Medtherm Schmidt-Boelters and the aluminum gauges are AEDC Schmidt-Boelters.

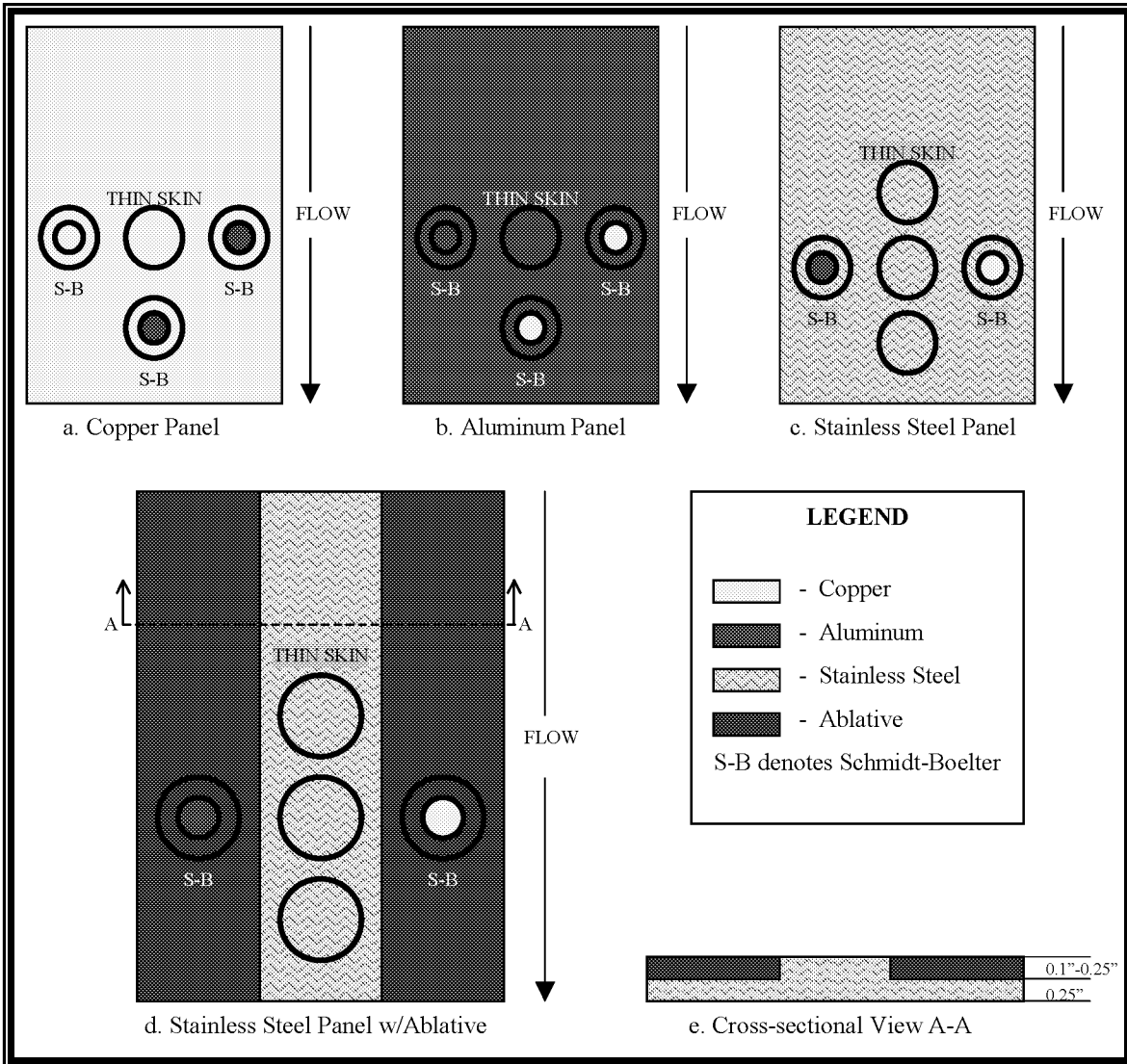


Figure 5: Testing Panel Configuration

The primary purpose of the study is determine dissimilar material effects, and the testing will be used for model calibration, that will build confidence for use of the models to correct in-flight data. In addition, the impact of gage/wafer orientation with respect to convective flow direction will also be studied in the testing program. The testing matrix shown in Table 1 (Page 7) also includes a couple of radiant test points that will eliminate thermal boundary layer effects and allow focus on radial heat transfer effects.

Table 1: Basic Testing Matrix

Test # (by priority)	Panel	Angle	Approx. HR (Btu/h ² /s)	Comments	Time (s)
1	Stainless Steel Plate	0°	4.7	Baseline	20
2	Stainless Steel Plate	0°	4.7	Repeat Baseline	20
3	Aluminum Plate	0°	4.7	Baseline	20
4	Aluminum Plate	0°	4.7	Repeat Baseline	20
5	BTA/SS/Hypalon	0°	4.7	Baseline	20
6	BTA/SS/Hypalon	0°	4.7	Repeat Baseline	20
7	Copper Plate	0°	4.7	Baseline	20
8	Copper Plate	0°	4.7	Repeat Baseline	20
9	Stainless Steel Plate	0°	4.7	Baseline with Medtherm calorimeters rotated 120°	20
10	Stainless Steel Plate	0°	4.7	Repeat Baseline with Medtherm calorimeters rotated 120°	20
11	Stainless Steel Plate	0°	4.7	Baseline with Medtherm calorimeters rotated 240°	20
12	Stainless Steel Plate	0°	4.7	Repeat Baseline with Medtherm calorimeters rotated 240°	20
13	BTA/SS/Hypalon	TBD	8.0	Baseline	20
14	BTA/SS/Hypalon	TBD	8.0	Repeat Baseline	20
15	BTA/SS/Hypalon	0°	4.7	Baseline, radiant	20
16	BTA/SS/Hypalon	0°	4.7	Repeat Baseline, radiant	20
17	Aluminum Plate	0°	4.7	Baseline with Medtherm calorimeters rotated 120°	20
18	Aluminum Plate	0°	4.7	Repeat Baseline with Medtherm calorimeters rotated 120°	20
19	Aluminum Plate	0°	4.7	Baseline with Medtherm calorimeters rotated 240°	20
20	Aluminum Plate	0°	4.7	Repeat Baseline with Medtherm calorimeters rotated 240°	20
21	Copper Plate	0°	4.7	Baseline with Medtherm calorimeters rotated 120°	20
22	Copper Plate	0°	4.7	Repeat Baseline with Medtherm calorimeters rotated 120°	20
23	Copper Plate	0°	4.7	Baseline with Medtherm calorimeters rotated 240°	20
24	Copper Plate	0°	4.7	Repeat Baseline with Medtherm calorimeters rotated 240°	20

In addition to the usual IHGF measurements and the thin skin and S-B data, surface IR (Infrared) data will be important. Spot IR and surface plane IR data will be used to determine the surface temperature profile of the plate, focusing on the areas on and in the near vicinity of the S-B gauges. This information will be crucial in the model calibration efforts, especially for determining the boundary layer effects caused by the surface temperature differences between the panel and the S-B gauges.

Finally, it will be important to understand the contact resistances between the S-B gauges and the surrounding material. The easiest way to establish this is by making the contact resistance as close to zero as possible using high conductivity thermal grease for the panels with no TPS.

POST-TEST MODEL ANALYSIS

As mentioned previously, the primary goal of this study is to correct and better understand in-flight measurements of heat fluxes on launch vehicles. Test data from the aerothermal facility will be used to calibrate the analytical models. In addition, a sensitivity analysis will be performed to determine the impact of sensor orientation, wafer thickness, epoxy thickness, and contact conductance from the sensor to the surrounding material. Also, during manufacturing, several deviances from production specifications can occur. For instance, the thermopile beads could be separated unevenly, they may not be centered, etc. The sensitivity analysis will investigate all of these types of variables and the effects they induce on the overall gauge measurement.

CONCLUSIONS

A three part program has been assembled that will produce a calibrated technique to correct material dissimilarity induced errors for in-flight Schmidt-Boelter heat flux measurements on launch vehicles. In general, the need for such corrections is greatest for aerothermal heating measurements. Two coupled models have been developed, one correcting boundary layer effects stemming from near step changes in the temperature from the surrounding material to the gauge, and the other accounting for radial heating errors. Testing in an aerothermal facility will provide the calibration. While this approach is more crucial to aerothermal heating measurements, the radial conduction effects model can also be applied to radiative measurement corrections, such as for plume radiation. While current uncorrected data provide conservative factors of safety, there are potential benefits attainable from reduced conservatism via lower TPS mass and reduced TPS application requirements.

ACKNOWLEDGEMENTS

The author(s) wish to acknowledge the help of the people at the MSFC Improved Hot Gas Facility, who have entered into a cooperative effort with us to obtain the necessary calibration data. Their assistance in fabricating the test panels and interfacing with heat flux gauge manufacturers and calibrators has been invaluable.

REFERENCES

1. Reynolds, W. C., Kays, W. M., and Kline, S. J., "Heat Transfer in the Turbulent Incompressible Boundary Layer, II – Step Wall-Temperature Distribution," in *NASA Memorandum*, Washington, NASA, 1958, pp. 1-3.
2. Rubesin, Morris W., "The Effect of an Arbitrary Surface-Temperature Variation along a Flat Plate on the Convective Heat Transfer in an Incompressible Turbulent Boundary Layer," in *NACA Technical Note 2345*, Moffett Field, CA, NACA, 1951, pp. 1-3, 24.

3. Westkaemper, John C., "On the Error in Plug-Type Calorimeters Caused by Surface-Temperature Mismatch," *Journal of the Aerospace Sciences*, November 1961, pp. 907-908.
4. Knox, E.C., "A Critique on Correcting Heat-Transfer Results for Temperature Mismatch," in *Remtech Inc. Technical Note RTN 158-02*, March 1987.
5. Kidd, C. T., "A Durable, Intermediate Temperature, Direct Reading Heat Flux Transducer for Measurements in Continuous Wind Tunnels," in *AEDC-TR-81-19*, Arnold AFS, TN, AEDC, 1981, pp. 7-15.
6. Kidd, C. T., "Thin-Skin Technique Heat-Transfer Measurement Errors Due to Heat Conduction into Thermocouple Wires," *ISA Transactions* **24**, no. 2, 1985, pp. 1-9.

CONTACT

Dr. Reinarts can be reached at the following e-mail address: Thomas.reinarts-1@ksc.nasa.gov.

NOMENCLATURE, ACRONYMS, ABBREVIATIONS

M	Mach Number
Re	Reynolds Number
T_{∞}	Free Stream Temperature
$T_{w1,w2}$	Wall Temperature
L	Running Length to Heat Flux Gauge
R	Radius of Heat Flux Gauge
W	$L+2R$
q''	Incident Heat Flux
δT	Differential Temperature
δx	Differential Length
TPS	Thermal Protection System
KSC	Kennedy Space Center
MSFC	Marshall Space Flight Center
IHGF	Improved Hot Gas Facility
AEDC	Arnold Engineering Development Center
S-B	Schmidt-Boelter
CFD	Computational Fluid Dynamics
k_f	Fluid thermal conductivity
∇T_{f0}	Temperature gradient of the fluid at the fluid wall interface
BTA	Low Conductivity Ablative
IR	Infrared